High power compatible internally sensed optical phased array

Lyle E. Roberts,[1,2,*] Robert L. Ward,[1,2] Samuel P. Francis,[1,2] Paul G. Sibley,[1,2] Roland Fleddermann,[1] Andrew J. Sutton,[1] Craig Smith,[2,3] David E. McClelland,[1], and Daniel A. Shaddock[1,2]

[1]*Department of Quantum Science, Research School of Physics and Engineering, The Australian National University, Canberra, ACT 2601, Australia*
[2]*Space Environment Research Centre (SERC), Advanced Instrumentation and Technology Centre, Mount Stromlo Observatory, Weston Creek, ACT 2611, Australia*
[3]*EOS Space Systems Pty Ltd, EOS House, Mount Stromlo Observatory, Weston Creek, ACT 2611, Australia*
[*]*Lyle.Roberts@anu.edu.au*

Abstract: The technical embodiment of the Huygens-Fresnel principle, an optical phased array (OPA) is an arrangement of optical emitters with relative phases controlled to create a desired beam profile after propagation. One important application of an OPA is coherent beam combining (CBC), which can be used to create beams of higher power than is possible with a single laser source, especially for narrow linewidth sources. Here we present an all-fiber architecture that stabilizes the relative output phase by inferring the relative path length differences between lasers using the small fraction of light that is back-reflected into the fiber at the OPA's glass-air interface, without the need for any external sampling optics. This architecture is compatible with high power continuous wave laser sources (e.g., fiber amplifiers) up to 100 W per channel. The high-power compatible internally sensed OPA was implemented experimentally using commercial 15 W fiber amplifiers, demonstrating an output RMS phase stability of $\lambda/194$, and the ability to steer the beam at up to 10 kHz.

OCIS codes: (060.2320) Fiber optics amplifiers and oscillators; (140.3298) Laser beam combining; (120.3180) Interferometry; (120.5050) Phase measurement.

References and links

1. R.G. Smith, "Optical power handling capacity of low loss optical fibers as determined by stimulated Raman and Brillouin scattering," Appl. Opt. **11**(11), 2489–2494 (1972).
2. J. Mason, J. Stupl, W. Marshall, and C. Levit, "Orbital debris–debris collision avoidance," Adv. Space Res. **48**(10), 1643–1655 (2011).
3. H. Brueselbach, S. Wang, M. Minden, D.C. Jones, and M. Mangir, "Power-scalable phase-compensating fiber-array transceiver for laser communications through the atmosphere," J. Opt. Soc. Am. B. **22**(2), 347–353 (2005).
4. P.F. McManamon, T.A. Dorschner, D.L. Corkum, L.J. Friedman, D.S. Hobbs, M. Holz, S. Liberman, H.Q. Nguyen, D.P. Resler, and R.C. Sharp, "Optical phased array technology," Proc. IEEE **84**(2), 268–298 (1996).
5. T.M. Shay, V. Benham, J.T. Baker, B. Ward, A.D. Sanchez, M.A. Culpepper, D. Pilkington, J. Spring, D.J. Nelson, and C.A. Lu, "First experimental demonstration of self-synchronous phase locking of an optical array," Opt. Express **14**(25), 12015–12021 (2006).
6. C.X. Yu, S.J. Augst, S.M. Redmond, K.C. Goldizen, D.V. Murphy, A. Sanchez, and T.Y. Fan, "Coherent combining of a 4 kw, eight-element fiber amplifier array," Opt. Lett. **36**(14), 2686–2688 (2011).

#262846 Received 12 Apr 2016; accepted 27 May 2016; published 9 Jun 2016

7. G.S. Goodno, S.J. McNaught, J.E. Rothenberg, T.S. McComb, P.A. Thielen, M.G. Wickham, and M.E. Weber, "Active phase and polarization locking of a 1.4 kW fiber amplifier," Opt. Lett. **35**(10), 1542–1544 (2010).
8. M.A. Vorontsov, S.L. Lachinova, L.A. Beresnev, and T. Weyrauch, "Obscuration-free pupil-plane phase locking of a coherent array of fiber collimators," J. Opt. Soc. Am. A **27**(11), A106–A121 (2010)
9. D.J. Bowman, M.J. King, A.J. Sutton, D.M. Wuchenich, R.L. Ward, E.A. Malikides, D.E. McClelland, and D.A. Shaddock, "Internally sensed optical phased array," Opt. Lett. **38**(7), 1137–1139 (2013).
10. L.E. Roberts, R.L. Ward, A.J. Sutton, R. Fleddermann, G. de Vine, D.M.Wuchenich, E.A. Malikides, D.E. McClelland, and D.A. Shaddock, "Coherent beam combining using a 2D internally sensed optical phased array," Appl. Opt. **53**(22), 4881–4885 (2014).
11. D.A. Shaddock, "Digitally enhanced heterodyne interferometry," Opt. Lett., **32**(22), 3355–3357 (2007).
12. D. M. Wuchenich, T. Lam, J. H. Chow, D. E. McClelland, and D. A. Shaddock, "Laser frequency noise immunity in multiplexed displacement sensing," Opt. Lett. **36**(5), 672–674 (2011).
13. G. de Vine, D. S. Rabeling, B. J. Slagmolen, T. Y. Lam, S. Chua, D. M. Wuchenich, D. E. McClelland, and D. A. Shaddock, "Picometer level displacement metrology with digitally enhanced heterodyne interferometry," Opt. Exp. **17**(2), 828–837 (2009).
14. D.A. Shaddock, B. Ware, P. G. Halverson, R. E. Spero, and B. Klipstein, "Overview of the LISA phasemeter," AIP Conf. Proc. **873**, 654–660 (2006).
15. A. Kobyakov, M. Sauer, and D. Chowdhury, "Stimulated Brillouin scattering in optical fibers," Adv. Opt. Photonics **2**(1), 1–59 (2010).
16. B. Anderson, A. Flores, R. Holten, and I. Dajani, "Comparison of phase modulation schemes for coherently combined fiber amplifiers" Opt. Express **23**(21), 27046–27060 (2015).
17. A. Flores, C. Robin, A. Lanari, and I. Dajani, "Pseudo-random binary sequence phase modulation for narrow linewidth, kilowatt, monolithic fiber amplifiers," Opt. Express **22**(15), 17735–17744 (2014).
18. G.D. Goodno, C-C. Shih, and J.E. Rothenberg, "Perturbative analysis of coherent combining efficiency with mismatched lasers," Opt. Express **18**(24), 25403–25414 (2010).

1. Introduction

Optical phased arrays (OPAs) provide a way to scale optical power beyond the capabilities of conventional narrow linewidth continuous wave fiber lasers, which are typically limited by the onset of non-linear effects such as stimulated Brillouin scattering (SBS) [1]. They work by stabilizing the relative output phase of multiple, spatially separate optical fiber apertures to form a coherent optical wave-front in the far field. OPAs can also perform fast beam steering and forming by precisely controlling the output phase of individual emitters. This ability to perform fast beam-steering and forming, in addition to their scalability and high power handling capabilities make OPAs a promising technology for applications requiring coherent high intensity sources including ground based space debris tracking and maneuvering [2] and free-space optical communications [3]. A comprehensive review of OPA technology is provided in [4].

Coherent beam combination (CBC) requires the stabilization of the wave-front phase at the output of each element in the OPA. This typically involves measuring the phase of the output wave-front to actively compensate for any relative path length fluctuations between uncommon lengths of fiber. Almost all existing CBC techniques measure the output phase of the array by sampling the outgoing beam externally using free space optics (e.g., [5–8]). In contrast to external sensing, Bowman et al. [9] and Roberts et al. [10] presented a technique that does not require free-space optics to measure the output phase of the beam, instead relying on the small fraction of light that is reflected back into the fiber at the OPA's glass-air interface to infer the relative phase of each emitter. This internal sensing technique infers the differential phase between uncommon paths by measuring the phase of the back-reflected light that double-passes each fiber. The relative phase at the output of the array is then stabilized by actively controlling the path lengths of each fiber.

The output phase of each emitter is isolated and measured using digitally enhanced heterodyne interferometry (DEHI) [11], which employs spread-spectrum modulation techniques to discriminate individual reflections at a single detector, without sacrificing the sub-wavelength sensitivity of conventional heterodyne interferometry. DEHI works by exploiting the correlation properties of pseudo-random noise (PRN) codes that are phase modulated onto the carrier

#262846 Received 12 Apr 2016; accepted 27 May 2016; published 9 Jun 2016

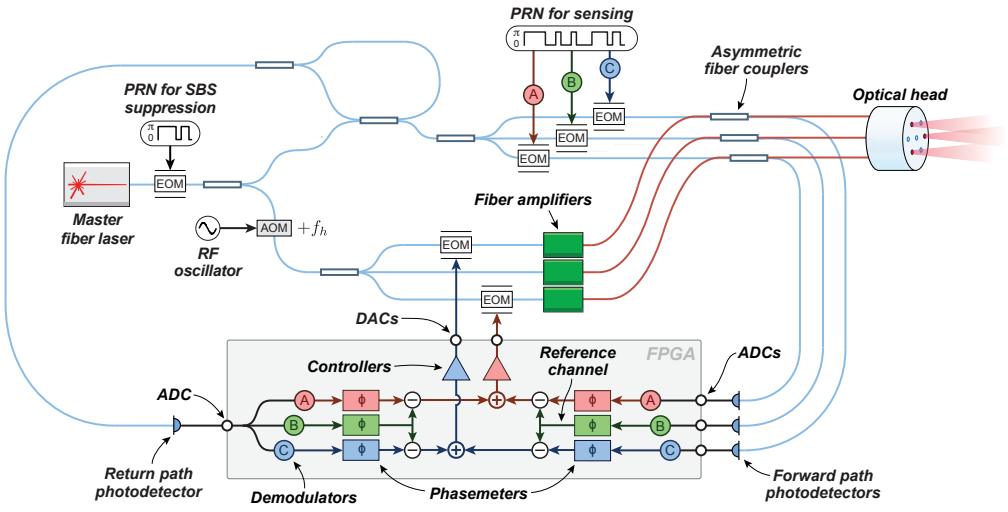

Fig. 1. Idealized fiber amplifier compatible internally sensed optical phased array.

electric field using an electro-optic modulator (EOM). Signals belonging to the various reflections in the optical system are then isolated by digitally demodulating the detected signal using correspondingly delay matched versions of the PRN code, suppressing contributions from other reflections.

Whilst the OPA design in [10] successfully validated the internal sensing concept, it also highlighted the architecture's incompatibility with in-line fiber amplifiers which do not tolerate back-reflected light. The total combined power of Roberts' OPA was limited to that of the master laser, and unable to support optical powers exceeding the damage threshold of sensitive optical devices (e.g., EOMs, which have a damage threshold on the order of $\sim$100 mW) in each path. In contrast, the OPA described here (shown in Fig. 1) overcomes both of these limitations, enabling it to operate at optical powers restricted only by the damage threshold of the asymmetric fiber couplers, and the onset of SBS in each emitter.

2. Amplifier compatible internally sensed optical phased array

The architecture of the proposed amplifier compatible internally sensed OPA is shown in Fig. 1, demonstrated using a three-emitter array. Light from a free-running laser is separated into two arms. The first (upper arm in the figure) is split into three channels, all of which are connected to $>$100 MHz fiber waveguide EOMs for PRN phase modulation. The second arm is frequency shifted by f_h using a fiber coupled acousto-optic modulator (AOM) and then split into three channels, each containing an EOM for feedback actuation, and a fiber amplifier.

Pairs of channels from the two arms are combined using commercial 99.9/0.1 asymmetric fiber couplers to form three Mach-Zehnder interferometers. The asymmetric fiber couplers are configured such that 0.1% of the amplified frequency shifted light interferes with 99.9% of the unshifted light at a high bandwidth forward path photodetector. The other 99.9% of the amplified frequency shifted light travels directly to the optical head where it propagates into free space. When light exits the OPA $\sim$4% is reflected back into the fiber due to Fresnel reflection. These reflections travel in the reverse direction back towards the asymmetric fiber couplers. 99.9% of the back-reflected light travels directly to the amplifiers where it is blocked by the amplifier's in-built optical isolator. The remaining 0.1% of the back-reflected light passes back

#262846 Received 12 Apr 2016; accepted 27 May 2016; published 9 Jun 2016

through the first arm, passing through the first series of EOMs where it is phase modulated with PRN before being interfered with an unshifted reference signal at a high-bandwidth return path photodetector.

The forward and return path photodetectors are necessary to sense the phase contributions of all uncommon optical path lengths in the optical system. A measurement of the phase in each optical path length allows us to stabilize the relative output phase of the OPA. The signal at each of the forward path detectors stems from the interference of the high-power and local oscillator paths, and has the form

$$s_{Fn}(t) = A_n \sin\left(\omega_h t + \Phi_{Fn} + \beta c(t-\tau_n)\right) \tag{1}$$

where the index n represents the channel number, A_n is the amplitude of the interference at the detector, ω_h is the angular heterodyne frequency, Φ_{Fn} is the phase, and β is the modulation depth of the binary PRN code $c(t-\tau_n) \in [0,1]$ delayed by τ_n. When the modulation depth $\beta = \pi$ we can use the identity $\sin(\theta \pm \pi) = -\sin(\theta)$ to simplify Eq. (1) using the equation $p(t-\tau) = 1 - 2c(t-\tau)$ to map $c(t) \in [0,1]$ to $p(t) \in [1,-1]$:

$$s_{Fn}(t) = p(t-\tau_n) A_n \sin\left(\omega_h t + \Phi_{Fn}\right)$$

The signal at the return path detector is the sum of the back-reflected signals $r_{Rk}(t)$ interfering with the local oscillator

$$\begin{aligned} s_{Rk}(t) &= \sum_k r_{Rk}(t) \\ &= \sum_k p(t-\tau_k) B_k \sin\left(\omega_h t + \Phi_{Rk}\right) \end{aligned}$$

where the index k indicates the channel number, B_k is the k'th channel's amplitude, and Φ_{Rk} represents the phase of channel k. A description of how an arbitrarily large number of PRN modulated signals incident on a single photodetector affects the signal-to-noise ratio of the phase measurement is presented in [12] and [13].

The signals at each detector are digitized using high bandwidth analog-to-digital converters (ADCs), and then digitally demodulated using a delay matched version of the code $p(t-\tau)$ corresponding to each channel in the OPA, exploiting the auto-correlation properties of PRN codes to suppress the contributions from other reflections. The phase of each demodulated signal is then measured using phase-locked loops (phasemeters) implemented digitally using a field-programmable gate-array (FPGA) [14]. FPGAs are inherently scalable and can support a large number of inputs and outputs.

3. Optical phase at the forward and return path photodetectors

The example two channel optical system shown in Figs. 2 and 3 illustrates the various phase contributions from each of the optical path lengths traveled by the light on the way to each detector. The phase measured at the two forward path detectors is:

$$\begin{aligned} \Phi_{F0} &= (\phi_0 + \phi_A) - (\phi_1 + \phi_2 + \phi_a) \\ \Phi_{F1} &= (\phi_0 + \phi_B) - (\phi_1 + \phi_2 + \phi_b) \end{aligned}$$

The phase of each channel measured at the return path detector is:

$$\Phi_{R0} = (\phi_0 + \phi_A + 2\phi_c + \phi_a + \phi_2 + \phi_R) - (\phi_1 + \phi_{LO}) \tag{2}$$

$$\Phi_{R1} = (\phi_0 + \phi_B + 2\phi_d + \phi_b + \phi_2 + \phi_R) - (\phi_1 + \phi_{LO}) \tag{3}$$

#262846 Received 12 Apr 2016; accepted 27 May 2016; published 9 Jun 2016

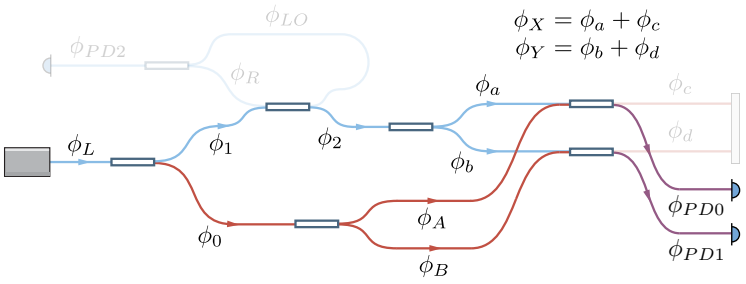

Fig. 2. Forward path phase contributions from each unique length of fiber in the optical system. For clarity only two fibers are shown.

If we apply feedback to lock the relative phase of forward paths at the asymmetric fiber couplers, in the high-gain limit we get

$$\hat{\Phi}_{F0} = (\phi_0 + \phi_A) - (\phi_1 + \phi_2 + \phi_a) = 0$$
$$\therefore (\phi_0 + \phi_A) = (\phi_1 + \phi_2 + \phi_a) \tag{4}$$
$$\hat{\Phi}_{F1} = (\phi_0 + \phi_B) - (\phi_1 + \phi_2 + \phi_b) = 0$$
$$\therefore (\phi_0 + \phi_B) = (\phi_1 + \phi_2 + \phi_b) \tag{5}$$

but this only stabilizes the relative path lengths up to the asymmetric coupler, and does not take into account the round-trip phase contributions $2\phi_c$ and $2\phi_d$. It is worth noting here that an alternative architecture with independent high power laser sources in place of the fiber amplifiers could be employed. These sources would similarly be phase-locked at the forward path detectors. The rest of the analysis applies to both cases.

Substituting Eqs. (4) and (5) into Eqs. (2) and (3) respectively provides the return path phase when the forward paths are locked:

$$\hat{\Phi}_{R0} = 2\phi_a + 2\phi_c + 2\phi_2 + \phi_R - \phi_{LO}$$
$$\hat{\Phi}_{R1} = 2\phi_b + 2\phi_d + 2\phi_2 + \phi_R - \phi_{LO}$$

The relative phase difference of the return path interferometers is then

$$\hat{\Phi}_{error} = (2\phi_b + 2\phi_d) - (2\phi_a + 2\phi_c)$$
$$= 2\phi_Y - 2\phi_X$$

where

$$\phi_X = \phi_a + \phi_c$$
$$\phi_Y = \phi_b + \phi_d$$

providing us with the information required to stabilize the remaining uncommon optical path lengths. By combining $\hat{\phi}_{error}$ with the forward path error signal $\hat{\Phi}_{F0}$ and $\hat{\Phi}_{F1}$ we can stabilize the relative path lengths of both channels:

$$\hat{\Phi}_{error,YX} = 2\phi_Y - 2\phi_X = 0$$
$$\therefore \phi_Y = \phi_X$$

#262846 Received 12 Apr 2016; accepted 27 May 2016; published 9 Jun 2016

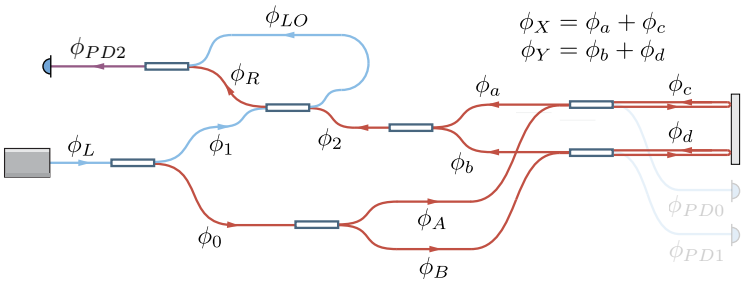

Fig. 3. Return path phase contributions from each unique length of fiber in the optical system. For clarity only two fibres are shown.

The same result applies for additional channels, for example a third channel ϕ_Z:

$$\hat{\Phi}_{error,ZX} = 2\phi_Z - 2\phi_X = 0$$
$$\therefore \phi_Z = \phi_Y = \phi_X$$

4. Feedback control

The control system used to stabilize the relative output phase of the OPA has two stages: i) forward path stabilization; and ii) return path stabilization. Feedback for the two control stages is actuated using a single EOM in each of the amplifier paths, which means we can use a single controller that accepts a linear combination of the forward and return path error signals to control the entire system (see Fig. 1). Feedback control can also be actuated using an AOM or piezo-electric fiber stretcher with only minor modification to the control system to account for the different transfer functions of both technologies.

The EOMs used to stabilize the optical path lengths have a limited actuation range of approximately ± 20 cycles, which can be extended by exploiting the 2π ambiguity of phase. A phase wrapping algorithm implemented at the output of each controller detects whenever the feedback signal exceeds two predefined thresholds and immediately wraps it by one cycle. The thresholds are padded to prevent rapid and repeated wrapping caused by noisy signals. The wrapping concept is illustrated in Fig. 4.

5. Linewidth broadening for SBS suppression

The primary motivation behind CBC is to overcome the limitations caused by non-linear effects like stimulated Brillouin scattering. Whilst OPAs overcome these limits by combining the power of multiple lasers, there are obvious advantages in maximizing the amount of power that can be delivered by each element in the array. An approximate expression for the SBS threshold power is [15]

$$P_{th} \approx 21 \frac{bA_e}{g_B L_e} \left(1 + \frac{\Delta\nu_L}{\Delta\nu_B}\right)$$

where b is a number between 1 and 2 depending on the polarization state of the laser, A_e is the effective mode area, g_B is the peak Brillouin gain for the dominant acoustic mode, L_e is the effective transmission length of the fiber, $\Delta\nu_L$ is the line width of the laser, and $\Delta\nu_B$ is the SBS interaction bandwidth. Options to increase P_{th} are to decrease the effective transmission length L_e, increase the effective mode area A_e, and increase the spectral line width of the laser $\Delta\nu_L$.

#262846 Received 12 Apr 2016; accepted 27 May 2016; published 9 Jun 2016

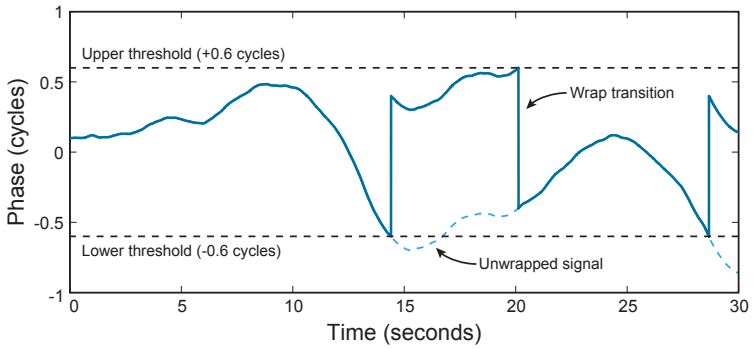

Fig. 4. Phase wrapping algorithm used to exploit the 2π ambiguity of phase. At $\sim$14 seconds the feedback signal encounters the lower threshold at -0.6 cycles. This prompts the wrapping algorithm to add 1 cycle to the feedback signal, which immediately jumps to +0.4 cycles.

Assuming that L_e can be minimized by design, and that large mode area optical fiber can be used to increase A_e, the remaining strategy is to broaden the linewidth of the laser, which can be achieved by modulating its phase with high-frequency pseudo-random noise to 'spread' the energy of the carrier frequency [16, 17].

This phased array architecture is compatible with linewidth broadening techniques for SBS suppression. To maintain coherent combination, the modulation must be common to all arms of the interferometer. This modulation can be applied using an EOM located directly after the master laser (cf. Fig. 1). Any macroscopic path length differences in the optical system will degrade the coherence of the combined beam, the extent of which depends on the root mean square (RMS) path length difference ΔL_{RMS} between channels and the specific auto-correlation properties of the code used. The binary auto-correlation of the maximal-length sequences used in this system is

$$A(\tau) = \begin{cases} 2^N - 1 & \text{for } \tau = 0, L, 2L, \cdots \\ -1 & \text{for any other } \tau \end{cases}$$

where N is the order of the sequence, $L = 2^N - 1$ is the sequence length, and τ is the delay relative to itself. Given a code modulation frequency f_{chip}, the wavelength of a single chip in the PRN code traveling in a medium with refractive index n is $L_{chip} = c/(nf_{chip})$ where c represents the speed of light in vacuum. Coherence degrades approximately linearly as the RMS path length error ΔL_{RMS} approaches $\pm L_{chip}$. Measurements performed by Anderson et al. show that fringe visibility degrades proportional to a Sinc function as the optical path length error increases, and re-coheres every code length due to the periodic nature of PRN [16]. Consequently, any path length errors greater than L_{chip} result in incoherent combination. The faster the modulation f_{chip}, the tighter the tolerance on ΔL_{RMS}. The maximum tolerable RMS path length error ΔL_{RMS} in our system is at worst 10% of L_{chip}. For a 1 GHz code this is 2 cm; a 1 GHz PRN modulation can potentially increase the SBS threshold by a factor of $\sim$10 [17].

6. Experimental demonstration

The high power compatible internally sensed OPA was demonstrated experimentally and characterized using the setup shown in Fig. 5. Three emitters have been simultaneously stabilized

#262846 Received 12 Apr 2016; accepted 27 May 2016; published 9 Jun 2016

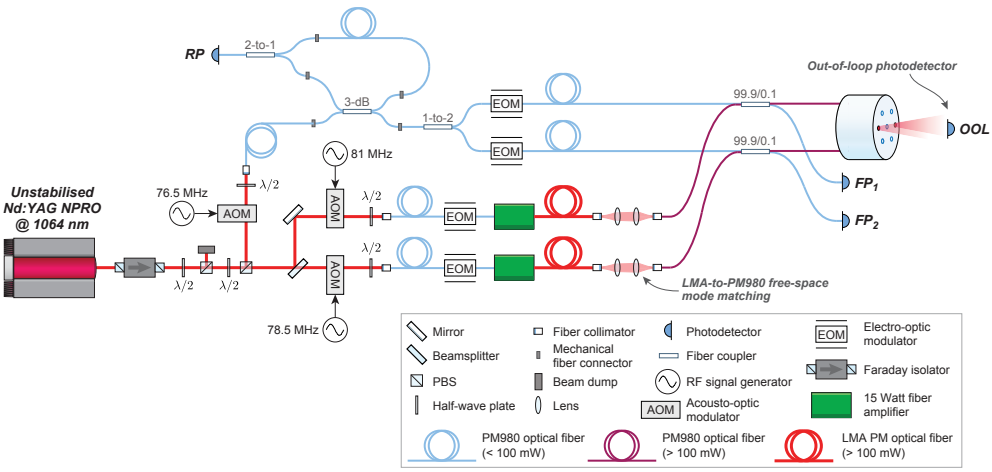

Fig. 5. Experimental configuration of the optical system used to characterize the high-power compatible internally sensed OPA.

and coherently combined. The fringe contrast was measured to be 99.8%, and, as expected, the peak intensity scales quadratically with number of emitters. We characterize the performance, however, by comparing the relative phase stability of two emitters at a time. In the following, we report results of an experiment to measure the RMS phase stability Φ_{RMS} between two emitters at the output of the OPA. SBS suppression via linewidth broadening will be tested in a future experiment.

Φ_{RMS} was measured using heterodyne detection by shifting the relative frequency of two emitters in the array, and then measuring the phase of the interference beat-note using a high-precision FPGA implemented phasemeter. Whilst this measurement introduces a frequency difference between the two emitters, the OPA's phase coherence is maintained. The measurement is performed out-of-loop (OOL) to capture the true relative phase error between the two emitters, as neither the forward- nor return-path photodetectors contain this information.

A free-space unstabilized Nd:YAG non-planar ring oscillator (NPRO) laser operating at 1064 nm was used as the master oscillator. Free-space AOMs were placed in the local oscillator and high-power arms to: 1) generate a heterodyne beat-note at the out-of-loop photodetector for direct measurement of the OPA's output phase stability; 2) allow the OPA to be locked *without* DEHI, providing a useful baseline from which to gauge what kind of effects DEHI has on Φ_{RMS}; and 3) prevent parasitic interference caused by the small fraction of zero-order unshifted light that couples with the first-order shifted light into the optical fiber. As mentioned in section 4, the AOMs in each of the amplified paths could be used to actuate feedback instead of the EOMs. In this experiment the AOMs are present for characterization purposes only.

Commercial 15 W fiber amplifiers were used in this experiment. They use steel-braided 10.5/125 μm (core diameter/cladding diameter) large mode area fiber to increase the SBS threshold. As our asymmetric fiber couplers (rated by the manufacturer to operate at up to 100 W continuous wave optical power) use standard 6/125 μm PM980 fiber, light was coupled from the amplifier's large mode area fiber to the coupler's PM980 fiber in free-space, requiring strict mode-matching optics for high-efficiency coupling. At least 90% coupling efficiency was achieved for each free-space link. The need for free-space coupling can be eliminated in the future by fusion splicing large mode area asymmetric fiber couplers directly to the amplifiers. Moving to large mode area fiber couplers may also overcome the 100 W per channel limit.

#262846 Received 12 Apr 2016; accepted 27 May 2016; published 9 Jun 2016

The heterodyne beat-note produced by the interference of the two emitters was detected using a commercial free-space 125 MHz bandwidth photodetector (labeled OOL in the figure), placed approximately 30 cm from the optical head. Equivalent fiber-coupled photodetectors were used to detect the interference at the return-path (RP) and forward-path (FP_1 and FP_2) photodetectors.

Without DEHI, the light from each channel is identified at FP_1, FP_2, and RP via RF demodulation. No cross-talk occurs between the 2 MHz and 4.5 MHz beat-notes present at the RP detector, as the phasemeters apply a band-pass filter with a bandwidth of a $\sim$100 kHz centered at the specific RF frequency.

The OOL phase was recorded at a rate of 31.250 kHz to preserve high-frequency harmonics. The time-series and root-power spectral density (RPSD) of the OOL measurements are shown *without* DEHI in Fig. 6. The same measurements performed *with* DEHI are shown in Fig. 7. Three measurements are presented in each figure: 1) when the OPA is unlocked (green); 2) when the forward path controllers are locked (blue); and 3) when both the forward and return path controllers are locked (magenta). The time series of Φ_{RMS} when both controllers are locked has been shifted to appear at zero phase for clarity. None of the time-series data has been detrended.

While unlocked, the OPA's output phase drifts around due to fiber noise (random fluctuations in optical path length and refractive index within the glass fiber) and laser frequency noise (coupled in by macroscopic differential path-length differences between the two paths in the Mach-Zehnder interferometer). The harmonics visible in the unlocked RPSD's between 10 Hz and 1 kHz originate from acoustic noise in the lab. Much of the acoustic noise is suppressed when the forward path controllers are engaged, which locks the relative phase of the amplified (lower) and local oscillator (upper) paths of the interferometer at their point of recombination at the asymmetric fiber couplers.

When the forward paths are locked the OOL phase error is limited primarily by fiber noise from the uncontrolled lengths of fiber between the asymmetric couplers and the optical head. The return-path controller stabilizes these uncontrolled lengths of fiber (magenta).

The RPSD of the fully stabilized output phase error shown in Fig. 6(b) reveals a white noise floor of 10 μCycles$/\sqrt{\text{Hz}}$ at frequencies between 10 Hz and 10 kHz. Whilst this noise-floor is higher than that of the forward path locked RPSD (blue), the RPSD demonstrates the RP controller's suppression of low-frequency fiber noise (at frequencies lower than 10 Hz). The 10 μCycles$/\sqrt{\text{Hz}}$ noise-floor of the fully locked RPSD is due to the low SNR of the RP signal, which limits the phasemeter's precision.

The RMS phase error for each measurement was calculated over a bandwidth of 15.625 kHz for a measurement period of 15 minutes. The RMS phase error without DEHI was calculated to be $\lambda/206$, limited at longer time scales by a low-frequency shelf at frequencies lower than 10 Hz. The RMS phase error with DEHI (with a $2^{24}-1$ bit long PRN code) is $\lambda/194$, limited primarily by harmonic distortion introduced by the imperfect demodulation of PRN in the controller. The harmonic distortion present in the DEHI measurements consists of peaks separated by 2.38 Hz, equal to the code-repetition rate of the $2^{24}-1$ element long PRN code: 40 MHz / $(2^{24}-1) = 2.38$ Hz. An RMS output phase error of $\lambda/194$ corresponds to a combination efficiency of $\eta \approx 99.9\%$, where $\eta \approx 1-\Delta\Phi^2_{RMS}$ [18].

The noise-shelf present below 10 Hz in both the fully locked traces is typical of cyclic phase noise, suggesting parasitic interference somewhere in the optical system. Quarter wave-plates were used to compensate for any polarization ellipticity, and a polarizer was placed in front of the OOL photodetector to reject orthogonal polarizations. Despite improving stability over very long time scales (>10,000 seconds), it did not significantly reduce the magnitude of the cyclic phase noise. The cyclic phase noise was, however, observed to be consistently lower when

#262846 Received 12 Apr 2016; accepted 27 May 2016; published 9 Jun 2016

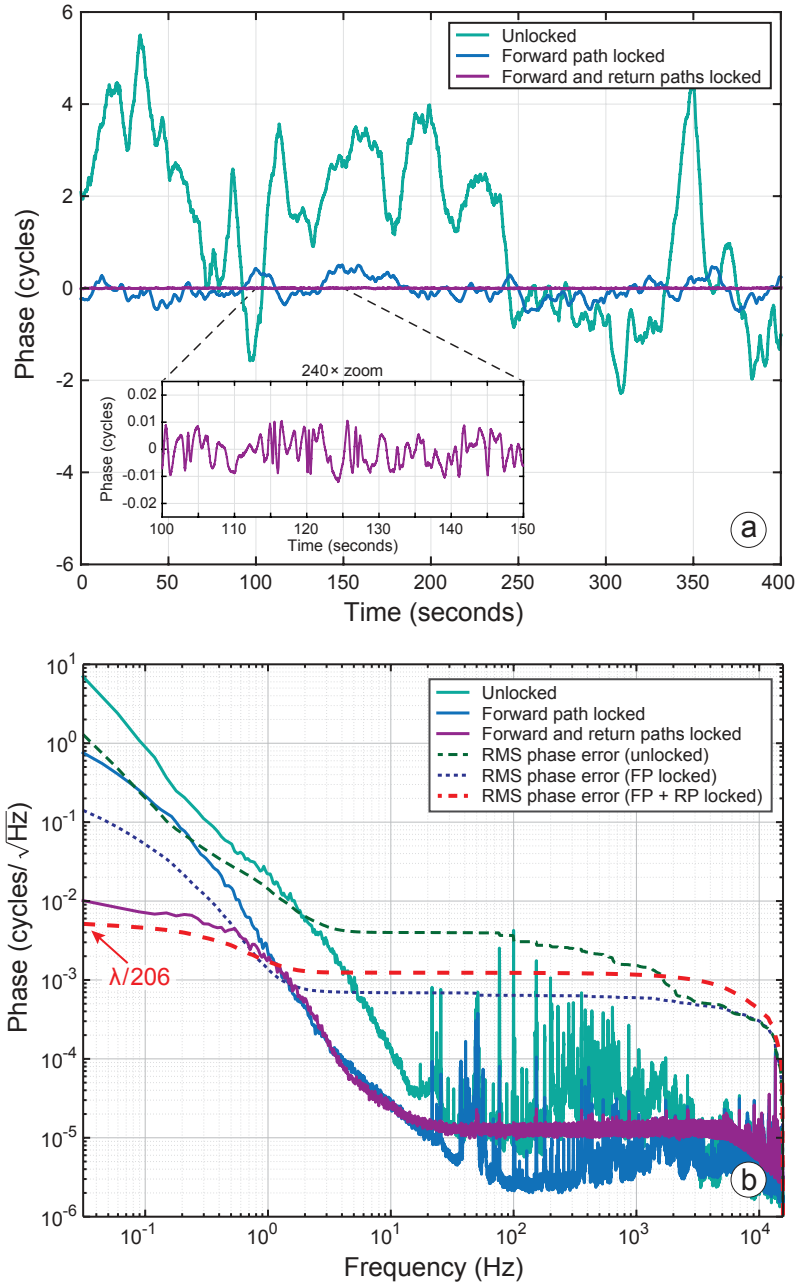

Fig. 6. (a) Time series measurements of Φ_{RMS} when the OPA is unlocked (green), forward-path locked (blue), and fully locked (magenta) without DEHI. The inset shows the zoomed-in behavior of Φ_{RMS}. (b) RPSD of the measurements shown in (a); the noise-shelf at frequencies below 10 Hz is typical of cyclic phase noise introduced by parasitic interference somewhere in the optical system.

#262846 Received 12 Apr 2016; accepted 27 May 2016; published 9 Jun 2016

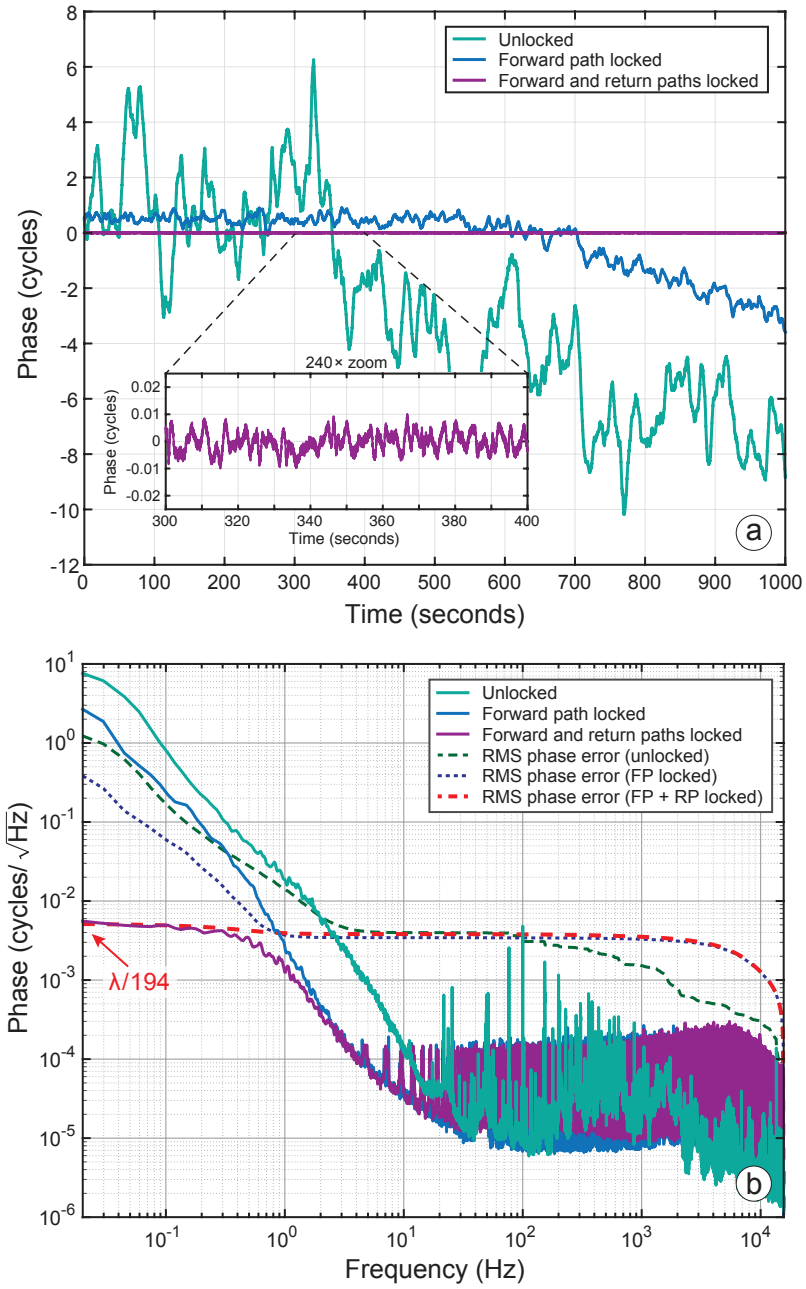

Fig. 7. (a) Time series measurements of Φ_{RMS} when the OPA is unlocked (green), forward-path locked (blue), and fully locked (magenta) *with* DEHI. The inset shows the zoomed-in behavior of Φ_{RMS}. (b) RPSD of the measurements shown in (a). The harmonic distortion visible on the forward and return path locked RPSD in (b) is caused by residual PRN noise introduced by the demodulator.

#262846 Received 12 Apr 2016; accepted 27 May 2016; published 9 Jun 2016

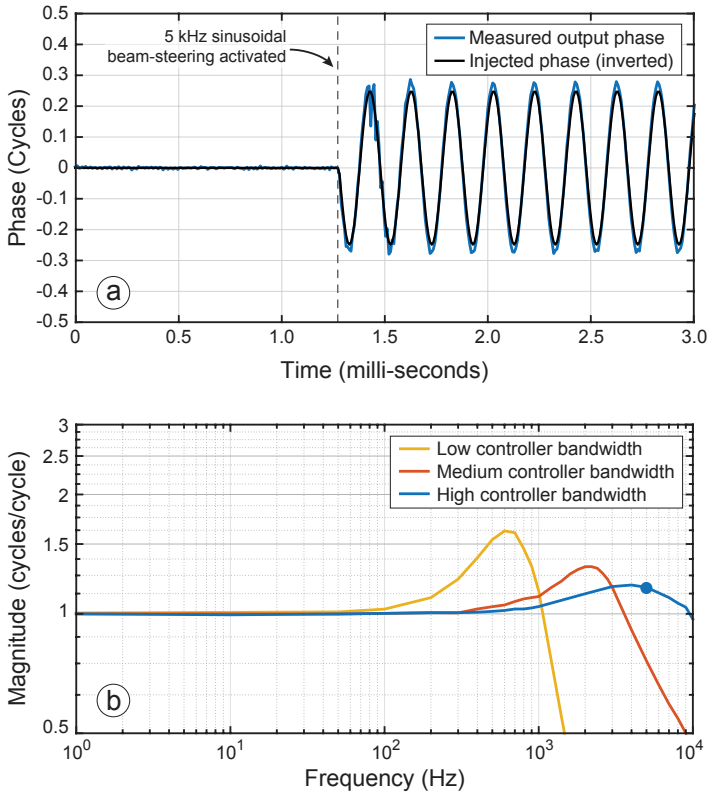

Fig. 8. (a) Time series measurement of 5 kHz sinusoidal beam-steering with a high controller bandwidth. (b) Measured magnitude response of beam-steering for different controller bandwidths. The 5 kHz tone shown in (a) is identified by the blue circle in (b).

using DEHI, suggesting partial suppression of the parasitic interference by DEHI's inherent range-gate [12].

Whilst the noise-shelf caused by cyclic phase noise is the highest magnitude feature in the RPSD, the results show that the it does not contribute that significantly to Φ_{RMS}. In the DEHI measurements, Φ_{RMS} is instead limited by residual phase noise introduced by imperfect demodulation of PRN.

7. Beam-steering

The distribution of optical power in the far-field can be manipulated by controlling the individual output phase of emitters in the OPA. One way to do this is to adjust the controller's zero point by adding an artificial phase shift to the error signal. The controller will attempt to correct any disturbances within its bandwidth, and will thus apply an equal and opposite magnitude phase shift to the light to suppress the error.

Dynamic beam-steering was demonstrated experimentally by adding a swept sine-wave (from 1 Hz up to 10 kHz) with an amplitude of 0.25 cycles to both the forward- and return-path phase measurements. This is equivalent to injecting a signal into the error point of the control loop; the control system then imposes this signal on the output. By comparing the injected signal to the measured phase at the OOL detector, we were able to calculate the beam-steering

#262846 Received 12 Apr 2016; accepted 27 May 2016; published 9 Jun 2016

forward-loop magnitude response. The OOL phase was measured using the setup shown in Fig. 5. The bandwidth of the phasemeter used to measure the phase of the OOL signal was set to 100 kHz.

Figure 8 shows a time series of the output and input phase measurements (upper panel), as well as the calculated magnitude response of the beam-steering for different controller bandwidths (lower panel). The results reveal the strong influence the controller bandwidth has over the range of frequencies the beam can be steered: higher controller bandwidths enable the controller to 'correct' higher frequency disturbances. At high controller bandwidths the beam can be steered by injecting into the forward- and return-path phasemeters up to approximately 10 kHz. The peaks clearly visible in all three magnitude response traces is caused by gain-peaking in the control loops.

The beam-steering bandwidth can in principle be extended by simultaneously injecting phase disturbances at frequencies higher than the controller bandwidth at the *output* of the controller, with appropriate blend filtering between the signals injected at the controller's input and output. These higher-frequency signals will not be suppressed by the controller as they exceed its bandwidth.

Whilst this demonstration of beam-steering was performed with two emitters, it is simple to extend the capability to an array of emitters with any topology. McManamon provides a detailed explanation of this in [4].

8. Conclusion

We have presented an architecture for an internally sensed optical phased array which overcomes limitations of previously reported internally sensed arrays—in particular the handling of high power. This design is fully scalable to a large number of emitters, each capable of delivering up to 100 W of continuous wave optical power limited only by the damage threshold of the commercial asymmetric fiber couplers. It may be possible in the future to extend the power handling capabilities of each emitter to kW levels using large mode area fiber taps. An experimental demonstration of the amplifier compatible OPA validated the concept, which was shown to stabilize the relative output phase of the array with an RMS phase error of $\lambda/194$ using digitally enhanced heterodyne interferometry. As the phase actuation is provided by high-bandwidth waveguide-based electro-optic modulators, it is possible to dynamically manipulate the distribution of optical power up to the bandwidth of the control system, enabling agile beam forming and steering. This system is also compatible with pseudo-random noise based linewidth broadening techniques for the suppression of stimulated Brillouin scattering. Use of a such a technique would result in a coherent phase-modulated beam that could be used for communications and ranging.

Acknowledgments

This research is supported by Australian Research Council Linkage Project 130101138 and the Cooperative Research Centre for Space Environment Management (SERC Limited) through the Australian Government's Cooperative Research Centre Programme. The authors thank Danielle Wuchenich and Nicolas Riesen for their insight and advice.

#262846 Received 12 Apr 2016; accepted 27 May 2016; published 9 Jun 2016